

Runtime-Assured, Real-Time Neural Control of Microgrids

Amol Damare Shouvik Roy Scott A. Smolka Scott D. Stoller

Stony Brook University, Stony Brook NY, USA

Abstract

We present *SimpleMG*, a new, provably correct design methodology for runtime assurance of microgrids (MGs) with neural controllers. Our approach is centered around the Neural Simplex Architecture, which in turn is based on Sha et al.’s Simplex Control Architecture. Reinforcement Learning is used to synthesize high-performance neural controllers for MGs. Barrier Certificates are used to establish SimpleMG’s runtime-assurance guarantees. We present a novel method to derive the condition for switching from the unverified neural controller to the verified-safe baseline controller, and we prove that the method is correct. We conduct an extensive experimental evaluation of SimpleMG using RTDS, a high-fidelity, real-time simulation environment for power systems, on a realistic model of a microgrid comprising three distributed energy resources (battery, photovoltaic, and diesel generator). Our experiments confirm that SimpleMG can be used to develop high-performance neural controllers for complex microgrids while assuring runtime safety, even in the presence of adversarial input attacks on the neural controller. Our experiments also demonstrate the benefits of online retraining of the neural controller while the baseline controller is in control.

1 Introduction

A *microgrid* (MG) is an integrated energy system comprising distributed energy resources (DERs) and multiple energy loads operating as a single controllable entity in parallel to, or islanded from, the existing power grid [27]. DERs tend to be *renewable* energy resources and include solar panels, wind turbines, batteries, and emergency diesel generators. By satisfying energy needs from local renewable energy resources, MGs can reduce energy costs and improve energy supply reliability for energy consumers.

Some of the major control requirements for an MG are active/reactive power control, load sharing, and frequency and voltage regulation. Control of MGs is challenging because MGs are complex systems subject to varying degrees of uncertainty, especially if a significant portion of the energy is provided by renewable DERs. Moreover, they are subject to various forms of disturbances, including short circuits, transients when DERs are connected or disconnected, and transients when the MG switches between grid-connected and islanded modes.

To help address these control challenges, the application of *neural networks for microgrid control* is on the rise [11]. Increasingly, Reinforcement learning (RL) is being used to train powerful Deep Neural Networks (DNNs) to produce high-performance MG controllers.

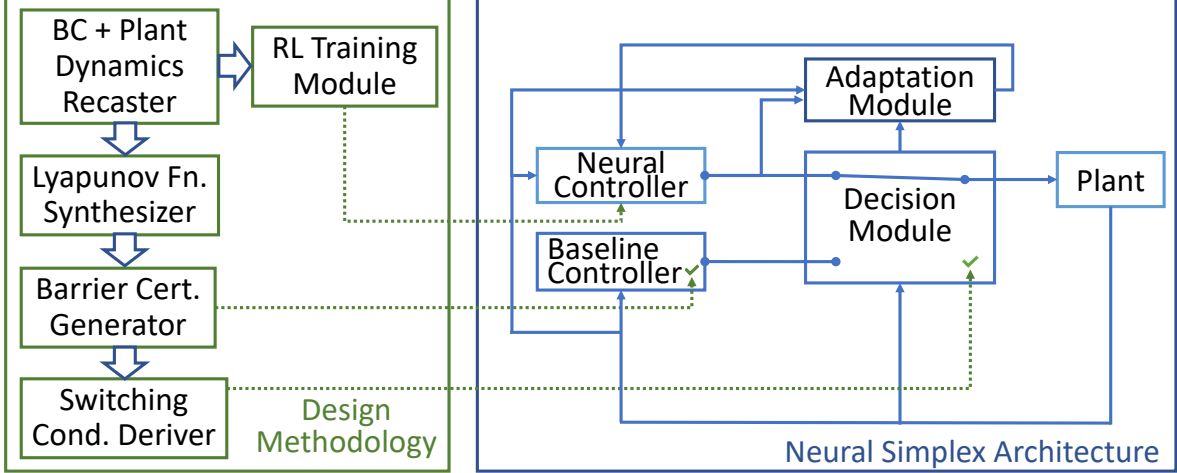


Figure 1: Overview of SimpleMG Runtime Assurance framework

In this paper, we present *SimpleMG*, a new, provably correct design methodology for runtime assurance of microgrids with neural controllers.¹ Our approach is centered around the Neural Simplex Architecture (NSA) [18], which in turn is based on Sha et al.’s Simplex Control Architecture [24, 25]. In NSA for MGs, an AI-based *neural controller* (NC), optimized for performance objectives such as power sharing and load balancing, is paired with a verified-safe *baseline controller* (BC), which maximizes stability and ensures overall system safety. A verified *decision module* (DM) *forward-switches* control from the NC to the BC when needed to ensure stability and safety, and *reverse-switches* from the BC to the NC to resume advanced control when appropriate. NSA also adds an *adaptation module* (AM) for online retraining of the NC.

Fig. 1 depicts the overall architecture of our proposed SimpleMG framework for microgrid control. The green box on the left outlines the Barrier Certificate (BaC)-based [21, 20] process we use to formally derive the switching conditions. First, we obtain the MG model dynamics, which is used for both deriving a Lyapunov function and for an RL training module. The Lyapunov function is used to generate a BaC, which provides the basis for our novel methodology for synthesizing a provably-safe forward switching condition (FSC). While prior approaches to FSC synthesis rely on online or offline reachability calculations, our methodology avoids reachability calculations, instead using a Taylor approximation of the BaC, and bounds on the BaC’s derivatives, to bound the possible values of the BaC during the next control period and thereby determine recoverability of states reachable during that time. Finally, RL training module is used to learn a high-performance NC. NSA for MGs is shown in blue box on the right.

We conducted an extensive experimental evaluation of SimpleMG using the RTDS high-fidelity, real-time digital simulation platform [23]. In particular, we considered an RTDS-based microgrid model [15] comprising three DERs: a battery, photovoltaic (PV, a.k.a. solar panels) and diesel generator. Our experiments, conducted in both grid-connected and islanded modes, demonstrate that our neural controller (NC) regulates the voltage faster than a traditional droop controller. Moreover, the overall error in voltage is smaller for the NC. NCs are also shown to be capable of

¹The name SimpleMG reflects the fact that our framework simplifies the process of developing safe and robust MGs and is intended to bring to mind the underlying Simplex control architecture.

generalization in terms of numbers of DERs and loads. We also experimentally demonstrated that our forward switching condition is not overly conservative, and that SimpleMG provides protection from adversarial inputs to the NC. In summary, the main contributions of this paper are the following:

- We present the SimpleMG design methodology for runtime-assured, real-time, neural control of microgrids.
- We develop a novel method based on Barrier Certificates to derive the (forward and reverse) switching logic underpinning SimpleMG, and prove the switching logic correct.
- We integrate SimpleMG with RTDS, a high-fidelity power systems simulator to achieve real-time MG control.
- We learn NCs that outperform traditional droop-based controllers.
- We show that RL-based NCs are vulnerable to adversarial inputs, and that SimpleMG offers protection and hardens the NC via online retraining.

The rest of the paper is organized as follows. Section 2 reviews the Neural Simplex Architecture framework. Section 3 discusses the baseline controller for the microgrid model as well as how we generate the Lyapunov functions. Section 4 shows our derivation of the switching conditions using barrier certificates. We also present our proof for the safety of NSA. Section 5 discusses the design of neural controllers using reinforcement learning. Section 6 focuses on the adaptation module and its support for online retraining. Section 7 showcases the results of our experimental evaluation. Section 8 considers related work. Section 9 offers our concluding remarks and directions for future research.

2 Background

The *Neural Simplex Architecture* (NSA) [18] is an approach to runtime assurance that provides safety guarantees for AI controllers of autonomous and other complex systems without sacrificing performance. NSA is inspired by Sha et al.’s Simplex control architecture [25, 24], where a pre-certified *decision module* (DM) switches control from a high-performance but unverified *advanced controller* (AC) to a verified-safe *baseline controller* (BC) if the AC produces an *unrecoverable action*, i.e., an action that could lead the system within one time step (i.e., one control period) to a state from which the BC is not guaranteed to preserve safety. NSA, like the original Simplex architecture, guarantees that safety of the plant is never violated.

The NSA portion of Fig. 1 (enclosed within the blue box) depicts the architecture’s main components. The high-performance Neural Controller (NC) is a DNN that takes the plant state as input and produces a control input for the plant as output. Unlike traditional Simplex’s view of the AC as a black box, NSA’s use of an NC allows online retraining of the NC by an *adaptation module* (AM). Online retraining is useful as it focuses the learning on areas of the state space that are relevant to the actual system behavior, i.e., regions of the state space the system actually visits. The AM seeks to eliminate unrecoverable actions from the NC’s behavior, without unduly degrading its performance, and in some cases actually improving its performance.

The BC is certified to guarantee that specified safety properties will hold provided it assumes control while the plant state is within a recoverable region \mathcal{R}_{BC} . A control input is *recoverable* in

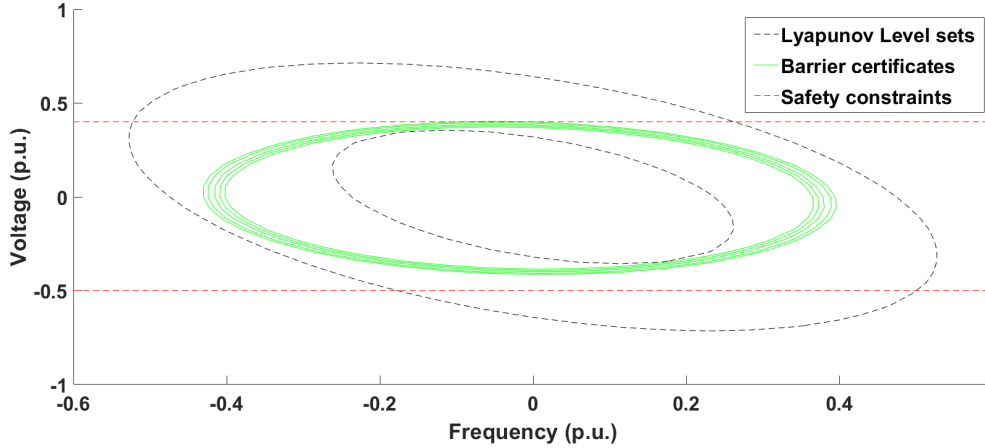


Figure 2: Lyapunov-function level sets (black-dotted ellipses). Innermost ellipse also indicates initial BaC, which is optimized iteratively (green ellipses). Red lines are voltage safety limits.

a given state if it keeps the plant inside \mathcal{R}_{BC} during the next time step. Otherwise, the control input is *unrecoverable* in that state. The DM forward-switches control to the verified-safe BC when the NC produces an unrecoverable control input. While the BC is in control, the AM retrains the NC. NSA also features reverse-switching from the BC to the NC.

3 Baseline Controller

3.1 Microgrid Control

An MG can operate in two modes: grid-connected and islanded. When operated in grid-connected mode, DERs act as constant source of power which can be injected into the network on demand. In contrast, in islanded or autonomous mode, the DERs form a grid of their own, meaning not only do they supply power to the local loads, but they also maintain the MG’s voltage and frequency within the specified limits [19]. The main objectives of MG control are voltage and frequency regulation and load sharing. In this paper, we focus on voltage regulation in both grid-connected and islanded modes. Specifically, we apply SimpleMG to the controller for the inverter for a Photovoltaic (PV) DER. Applying SimpleMG to other DERs which have inverter interfaces such as battery is straightforward. Of the three controllers necessary for diesel generator DER, our methodology can be applied to voltage and frequency controllers straightforwardly. The exciter system controls the magnetic flux flowing through the rotor generator, and its dynamics are coupled with that of the diesel engine. We plan to explore using the approach presented in [8] to handle these coupled dynamics and apply SimpleMG to the exciter system.

3.2 Droop Controller as Baseline Controller

We use a traditional droop controller as the baseline controller; see Fig. 1. Using the methodology described below, we derive a Barrier Certificate (BaC) to establish proof of the BC’s safety. This methodology is general enough to be applied to any type of controller. Consider the following

model of an MG's droop-controlled inverters

$$\dot{\theta}_i = \omega_i \quad (1a)$$

$$\dot{\omega}_i = \omega_i^0 - \omega_i + \lambda_i^p(\mathbf{P}_i - P_i) \quad (1b)$$

$$\dot{v}_i = v_i^0 - v_i + \lambda_i^q(\mathbf{Q}_i - Q_i) \quad (1c)$$

where θ_i , ω_i , and v_i are the phase angle, frequency, and voltage of the i^{th} inverter, respectively. \mathbf{P}_i and \mathbf{Q}_i are the inverter's active and reactive power set-points, and λ^p and λ^q are the droop controller's coefficients. The values of set-points \mathbf{P}_i and \mathbf{Q}_i of an inverter depend upon local loads and power needed by the rest of the MG. The loads are not explicitly modeled here. In our case studies, we vary these power set-points to simulate changing loads. Let \mathcal{M} be the set of all inverter indices. The active power P_i and reactive power Q_i are given by:

$$\begin{aligned} P_i &= v_i \sum_{j \in \mathcal{N}_i} v_k (G_{i,j} \cos \theta_{i,j} + B_{i,j} \sin \theta_{i,j}) \\ Q_i &= v_i \sum_{j \in \mathcal{N}_i} v_k (G_{i,j} \sin \theta_{i,j} - B_{i,j} \cos \theta_{i,j}) \end{aligned} \quad (2)$$

where $\theta_{i,j} = \theta_i - \theta_j$, and $\mathcal{N}_i \subseteq \mathcal{M}$ is the set of neighbors of inverter i . $G_{i,j}$ and $B_{i,j}$ are respectively the conductance and susceptance values of the transmission line connecting inverters i and j . As shown in [3], the stability of such a system can be verified using Lyapunov theory.

Our methodology for computing switching conditions (see Section 4) requires a BaC, but is independent of how the BaC is obtained. Currently we derive a Lyapunov function V for the system using the expanding interior-point algorithm in [3], and then use the SOS-based algorithm in [28, 9] to obtain a BaC from the Lyapunov function. Note that the largest super-level set of a Lyapunov function within a safety region is a BaC. The algorithm in [28, 9] computes a larger BaC by starting with that sub-level set and then expanding it, by allowing it to take shapes other than that of a sub-level set of the Lyapunov function. Fig. 2 shows this process of incrementally expanding the Lyapunov function to obtain the BaC. SOS-based algorithms apply only to polynomial dynamics, so we first recast droop controller dynamics to be polynomial using a DQ0 transformation [16] to AC waveforms. This transformation is exact; i.e., it does not introduce any approximation error. Other possible approaches to obtain polynomial dynamics are Taylor approximation [9] and the recasting techniques in [3].

Our methodology for deriving safety guarantees for the BC is as follows: (1) Obtain analytical dynamics for the plant + BC. (2) Convert non-polynomial dynamics to polynomial. (3) Compute a Lyapunov function for plant + BC using SOSTOOLS. (4) From the Lyapunov function, compute the BaC for plant + BC. Steps 3 and 4 involve a search of Lyapunov functions and BaCs of various degrees by choosing different candidate polynomials and parameters of SOS problem.

In our experimental evaluation (Section 7), we used this methodology to obtain BaCs for BCs in the form of droop controllers for voltage regulation, in the context of MGs containing up to three DERs of different types. Note that battery DERs operate in two distinct modes, charging and discharging, resulting in a hybrid system model with different dynamics in different modes. For now, we consider only runs in which the battery remains in the same mode for the duration of the run. Extending our framework to hybrid systems is future work.

4 Decision Module

The Decision Module (DM) implements the switching logic for both forward and reverse switching. When the forward-switching condition (FSC) is true, control is switched from the NC to the BC; likewise, when the reverse-switching condition (RSC) is true, control is switched from the BC to the NC. The success of our approach rests on solving the complex problems discussed in this section to derive an FSC.

Consider a continuous dynamical system of the form

$$\dot{x} = f(x, u) \quad (3)$$

where $x \in \mathbb{R}^k$ is the state of the plant at time t and $u \in \Omega$ is the control input provided to the plant at time t . The set of all valid control actions is denoted by Ω . The set of *unsafe states* is denoted by \mathcal{U} . Let $x_{lb}, x_{ub} \in \mathbb{R}^k$ be *operational bounds* on the ranges of state variables, reflecting physical limits and simple safety requirements. The set \mathcal{A} of *admissible states* is given by: $\mathcal{A} = \{x : x_{lb} \leq x \leq x_{ub}\}$. A state of the plant is *recoverable* if the BC can take over in that state and keep the plant invariably safe. For a given BC, we denote the *recoverable region* by \mathcal{R} . Note that \mathcal{R}_U and \mathcal{R} are disjoint. The safety of such system can be verified using BaC $h(x) : \mathbb{R}^k \rightarrow \mathbb{R}$ as defined in [21, 20, 28, 9]. of following form:

$$\begin{aligned} h(x) &\geq 0, \forall x \in \mathbb{R}^k \setminus \mathcal{U} \\ h(x) &< 0, \forall x \in \mathcal{U} \\ (\nabla_x h)^T f(x) + \sigma(h(x)) &\geq 0, \forall x \in \mathbb{R}^k \end{aligned} \quad (4)$$

where $\sigma(\cdot)$ is an extended class- \mathcal{K} function. The zero-super-level set of a BaC h is given by $\mathcal{Z}(h) = \{x : h(x) > 0\}$. [28] proves the invariance of this set and shows that $\mathcal{Z}(h) \subseteq \mathcal{R}$.

Let η denote the control period a.k.a. time step. Let $\hat{h}(x, u, \delta)$ denote the n^{th} -degree Taylor approximation of the BaC h 's value after time δ , if control action u is taken in state x . The approximation is computed at the current time to predict h 's value δ time units later and is given by $\hat{h}(x, u, \delta) = h(x, u) + \sum_{i=1}^n \frac{h^i(x, u)}{i!} \delta^i$, where $h^i(x, u)$ denotes the i^{th} time derivative of h evaluated in state x if control action u is taken. The control action is needed to calculate the time derivatives of h from the definition of h and Eq. 3 by applying the chain rule. Since we are usually interested in predicting the value one time step in the future, we define the shorthand $\hat{h}(x, u) = \hat{h}(x, u, \eta)$. By Taylor's theorem with the Lagrange form of the remainder, the remainder error of the approximation $\hat{h}(x, u)$ is: $\frac{h^{n+1}(x, u, \delta)}{(n+1)!} \eta^{n+1}$ for some $\delta \in (0, \eta)$. An upper bound on the remainder error, if the state remains in the admissible region during the time interval, is:

$$\lambda(u) = \left| \frac{\sup h^{n+1}(x)}{(n+1)!} \eta^{n+1} \right| : x \in \mathcal{A} \quad (5)$$

The FSC is based on checking recoverability during the next time step. For this purpose, the set \mathcal{A} of admissible states is shrunk by margins of μ_{dec} and μ_{inc} , a vector of upper bounds on the amount by which each state variable can decrease and increase, respectively, in one time step, maximized over all admissible states. Formally,

$$\begin{aligned} \mu_{\text{dec}}(u) &= |\min(0, \eta \dot{x}_{\min}(u))| \\ \mu_{\text{inc}}(u) &= |\max(0, \eta \dot{x}_{\max}(u))| \end{aligned} \quad (6)$$

where \dot{x}_{min} and \dot{x}_{max} are vectors of solutions to the optimization problems:

$$\begin{aligned}\dot{x}_i^{min}(u) &= \inf\{\dot{x}_i(x, u) : x \in \mathcal{A}\} \\ \dot{x}_i^{max}(u) &= \sup\{\dot{x}_i(x, u) : x \in \mathcal{A}\}\end{aligned}\tag{7}$$

The difficulty of finding these extremal values depends on the complexity of the functions $\dot{x}_i(x, u)$. For example, it is relatively easy if they are convex. In our case study of a realistic microgrid model, they are multivariate polynomials with degree 1 hence convex. The set \mathcal{A}_r of *restricted admissible states* is given by: $\mathcal{A}_r(u) = \{x : x_{lb} + \mu_{dec}(u) < x < x_{ub} - \mu_{inc}(u)\}$. Let $Reach_{=\eta}(x, u)$ denote the set of states reachable from state x after exactly time η if control action u is taken in state x . Let $Reach_{\leq\eta}(x, u)$ denote the set of states reachable from x within time η if control action u is taken in state x .

Lemma 1. *For all $x \in \mathcal{A}_r(u)$ and all control actions u , $Reach_{\leq\eta}(x, u) \subseteq \mathcal{A}$.*

Proof. The derivative of x is bounded by $\dot{x}_{min}(u)$ and $\dot{x}_{max}(u)$ for all states in \mathcal{A} . This implies that μ_{dec} and μ_{inc} are the largest amounts by which the state x can decrease and increase, respectively, during time η , as long as x remains within \mathcal{A} during the time step. Since $\mathcal{A}_r(u)$ is obtained by shrinking \mathcal{A} by μ_{dec} and μ_{inc} (i.e., by moving the lower and upper bounds, respectively, of each variable inwards by those amounts), the state cannot move outside of \mathcal{A} during time η . \square

4.1 Forward Switching Condition

To ensure safety, a forward-switching condition (FSC) should switch control from the NC to the BC if using the control action u proposed by NC causes any unsafe states to be reachable from the current state x during the next control period, or causes any unrecoverable states to be reachable at the end of the next control period. These two conditions are captured in the following definition:

Definition 1 (Forward Switching Condition). *A condition $FSC(x, u)$ is a forward switching condition if for every recoverable state x , every control action u , and control period η , $Reach_{\leq\eta}(x, u) \cap \mathcal{U} \neq \emptyset \vee Reach_{=\eta}(x, u) \not\subseteq \mathcal{R}$ implies $FSC(x, u)$ is true.*

Theorem 1. *A Simplex architecture whose forward switching condition satisfies Definition 1 keeps the system invariably safe, provided system starts in a recoverable state.*

Proof. Our definition of an FSC is based directly on the switching logic in Algorithm 1 of [30]. The proof of Theorem 1 of [30] shows that an FSC that is exactly the disjunction of the two conditions in our definition invariantly ensures system safety. It is easy to see that any weaker FSC also ensures safety. \square

We now propose a novel and general construction of a switching condition from a BaC and prove its correctness.

Theorem 2. *Given a barrier certificate h , the following condition is a forward switching condition: $FSC(x, u) = \alpha \vee \beta$ where $\alpha \equiv \hat{h}(x, u) - \lambda(u) \leq 0$ and $\beta \equiv x \notin \mathcal{A}_r(u)$*

Proof. Intuitively, $\alpha \vee \beta$ is an FSC because (1) if condition α is false, then control action u does not lead to an unsafe or unrecoverable state during the next control period, provided the state remains admissible during that period, and (2) if condition β is false, then the state will remain admissible

during that period. Thus, if α and β are both false, then nothing bad can happen during the control period, and there is no need to switch to the BC.

Formally, suppose x is a recoverable state, u is a control action, and $Reach_{\leq \eta}(x, u) \cap \mathcal{U} \neq \emptyset \vee Reach_{=\eta}(x, u) \not\subseteq \mathcal{R}$, i.e., there is an unsafe state in $Reach_{\leq \eta}(x, u)$ or an unrecoverable state in $Reach_{=\eta}(x, u)$. Let x' denote that unsafe or unrecoverable state. Recall that $\mathcal{Z}(h) \subseteq \mathcal{R}$, and $\mathcal{R} \cap \mathcal{U} = \emptyset$. Therefore, $h(x', u) \leq 0$. We need to show that $\alpha \vee \beta$ holds. We do a case analysis based on whether x is in $\mathcal{A}_r(u)$.

Case 1: $x \in \mathcal{A}_r(u)$. In this case, we use a lower bound on the value of the BaC h to show that states reachable in the next control period are safe and recoverable. Using Lemma 1, we have $Reach_{\leq \eta}(x, u) \subseteq \mathcal{A}$. This implies that $\lambda(u)$, whose definition maximizes over $x \in \mathcal{A}$, is an upper bound on the error in the Taylor approximation $\hat{h}(x, u, \delta)$ for $\delta \leq \eta$. This implies that $\hat{h}(x, u) - \lambda(u)$ is a lower bound on value of BaC for all states in $Reach_{\leq \eta}(x, u)$. As shown above, there is a state x' in $Reach_{\leq \eta}(x, u)$ with $h(x', u) \leq 0$. $\hat{h}(x, u) - \lambda(u)$ is lower bound on $h(x', u)$ and hence must also be less than or equal to 0. Thus, α holds.

Case 2: $x \notin \mathcal{A}_r(u)$. In this case, β holds. Note that in this case, the truth value of α is not significant (and not relevant, since $FSC(x, u)$ holds regardless), because the state might not remain admissible during the next control period, hence the error bound obtained using Eq. 5 is not applicable. \square

4.2 Reverse Switching Condition

The RSC is designed with a heuristic approach, since it does not affect safety of the system. To prevent frequent switching between the NC and BC, we design the RSC to hold if the FSC is likely to remain false for at least m time steps, with $m > 1$. The RSC, like the FSC, is the disjunction of two conditions. The first condition is $h(x) \geq m\eta|\dot{h}(x)|$, since h is likely to remain non-negative for at least m time steps if its current value is at least that duration times its rate of change. The second condition ensures that the state will remain admissible for m time steps. In particular, we take $RSC(x) = h(x) \geq m\eta|\dot{h}(x)| \wedge x \in \mathcal{A}_{r,m}$, where the m -times-restricted admissible region $\mathcal{A}_{r,m}$ is $\mathcal{A}_{r,m} = \{x : x_{lb} + m\mu_{dec} < x < x_{ub} - m\mu_{inc}\}$, where vectors μ_{dec} and μ_{inc} are defined in same way as $\mu_{dec}(u)$ and $\mu_{inc}(u)$ in Eqs. 6 and 7 except with optimization over all control actions u . An RSC that guarantees absence of forward switches for at least m time steps can be designed by using the maximum of $\dot{h}(x)$ over the admissible region; however, this conservative approach might leave the BC in control longer than desired.

4.3 Decision Logic

The DM's switching logic has three inputs: the current state x , the control action u currently proposed by the NC, and the name c of the controller currently in control (as a special case, we take $c = NC$ in the first time step). The switching logic is defined by cases as follows: $DM(x, u, c)$ returns BC if $c = NC \wedge FSC(x, u)$, returns NC if $c = BC \wedge RSC(x)$, and returns c otherwise.

5 Neural Controller

We present our approach for learning neural controllers (NCs) in the form of DNNs representing deterministic control policies. Such a DNN maps system states (or raw sensor readings) to control inputs. We use RL in form of Deep Deterministic Policy Gradient (DDPG) algorithm, with the

safe learning strategy of penalizing unrecoverable actions [18]. DDPG was chosen because it works with deterministic policies and is compatible with continuous action spaces.

5.1 Deep Deterministic Policy Gradient Algorithm

We consider a standard Reinforcement Learning setup consisting of an agent interacting with an environment in discrete time. At each time step t , the agent receives a (microgrid) state x_t as input, takes an action a_t , and receives a scalar reward r_t . An agent's behavior is defined by a policy that maps states to a probability distribution over the actions. The goal of Reinforcement Learning is to learn a policy that maximizes the reward function r from the starting state distribution J . Reward function r is an incentive mechanism that tells the agent what actions it should take (in terms of performance and safety) and, conversely, which ones it should avoid, using rewards and penalties.

The DDPG algorithm is a model-free, off-policy Reinforcement Learning method. *Model-free* means that the algorithm does not have access to a model of the environment (in our case, the microgrid dynamics). While model-free methods forego the potential gains in sample efficiency from using a model, they tend to be easier to implement and tune. An *off-policy* learner learns the value of the optimal policy independently of the current learned policy. A major challenge of learning in continuous action spaces is exploration. An advantage of off-policy algorithms such as DDPG is that the problem of exploration can be treated independently from the learning algorithm [10].

Off-policy learning is advantageous in our setting because it enables the NC to be (re-)trained using actions taken by the BC rather than the NC or the learning algorithm. The benefits of Off-policy retraining are further considered in Section 6.

The DDPG algorithm employs an *actor-critic framework*. The actor generates a control action and the critic evaluates its quality. The Actor network representing the actor is a DNN which in our case takes the vector state of the DER voltages and currents as its input, and outputs a continuous action $a_t = \mu(x_t|\theta^\mu)$, where θ^μ is the weight of the actor network. The Critic network representing the critic is a DNN that receives a state x_t and an action $\mu(x_t|\theta^\mu)$ as input, and produces a scalar Q -value. In order to learn from prior knowledge, DDPG uses a replay buffer R to store training samples of the form (x_t, a_t, r_t, x_{t+1}) , where x_t is the state at time t , a_t is the action taken at time t , r_t is the reward associated with the current state and action, and x_{t+1} is the next state.

At every training iteration, a set \mathcal{S} of samples is randomly chosen from the replay buffer. As such, \mathcal{S} is not necessarily generated using the current policy, but rather by the policies the DNN learned at different stages of training. Hence, DDPG is an off-policy algorithm. The critic agent $Q(x, a|\theta^Q)$ for each state x , where θ^Q is the weight of the critic agent, is updated using the Bellman equation. The actor policy is updated iteratively by the following policy gradient:

$$\nabla_{\theta^\mu} J \approx \frac{1}{S} \sum_t \nabla_a Q(x, a|\theta^Q)|_{x=x_t, a=\mu(x_t)} \nabla_{\theta^\mu} \mu(x|\theta^\mu)|_{x_t} \quad (8)$$

The critic network evaluates the action of the actor network based on its current reward. For further details regarding the implementation of the DDPG algorithm, please refer to Algorithm 1 [10].

To learn an NC for DER voltage control, we designed the following reward function, which guides the actor network to learn the desired control objective.

$$r(x_t, a_t) = \begin{cases} -1000 & \text{if FSC}(x_t, a_t) \\ 100 & \text{if } v_{t+1}^i \in [v_{ref} - \epsilon, v_{ref} + \epsilon] \\ -w \cdot (v_{t+1}^i - v_{ref})^2 & \text{otherwise} \end{cases} \quad (9)$$

where w is a weight, v_{t+1} is the DER voltage computed using the current action, v_{ref} is the reference or nominal voltage, and ϵ is the tolerance threshold. We assign a high negative reward for triggering the FSC, and a high positive reward for reaching the tolerance region, i.e., $v_{ref} \pm \epsilon$. The third clause rewards actions that lead to a state in which the DER voltage is close to its reference value.

5.2 Adversarial Inputs

Controllers obtained via deep RL algorithms are vulnerable to *adversarial inputs* (AIs): those that lead to a state in which the NC produces an unrecoverable action, even though the NC behaves safely on very similar inputs. NSA provides a defense against these kinds of attacks. If the NC proposes a potentially unsafe action, the BC takes over in a timely manner, thereby guaranteeing the safety of the system. To demonstrate NSA’s resilience to AIs, we use a gradient-based attack algorithm [17] to construct such inputs, and show that the DM switches control to the BC in time to ensure safety.

The gradient-based algorithm takes as input the critic network, actor network, adversarial attack constant c , parameters a, b of beta distribution $\beta(a, b)$, and the number of times n noise is sampled. For a given (microgrid) state x , the critic network is used to ascertain its Q -value and the actor network determines its optimal action. Once the gradient of the critic network’s loss function is computed using the Q -value and the action, the l_2 -constrained norm of the gradient ($grad_dir$) is obtained. An initial (microgrid) state x_0 , to be provided as input to the actor network, is then perturbed to obtain a potential adversarial state x_{adv} , determined by the sampled noise in the direction of the gradient: $x_{adv} = x_0 - c \cdot \beta(a, b) \cdot grad_dir$.

We can now compute the Q -value of x_{adv} and its (potentially adversarial) action a_{adv} . If this value is less than $Q(x_0, a_0)$, then x_{adv} leads to a sub-optimal action. A sub-optimal action, however, does not necessarily guarantee that the FSC will be triggered. Thus, we iterate the procedure n times in an attempt to find an adversarial state that produces an action that triggers the FSC.

Note that the gradient-based attack algorithm does not guarantee the successful generation of AIs every time it is executed, as this largely depends on the quality of the training (e.g., the training error) of the NC: the higher the quality of training, the lower the success rate of generating AIs. In our experiments (see Section 7.4), the highest rate of AI generation we observed is 0.008%.

6 Adaptation Module

The Adaptation Module (AM) retrains the NC in an online manner when the NC produces an unrecoverable action that causes the DM to failover to the BC. With retraining, the NC is less likely to repeat the same or similar mistakes in the future, allowing it to remain in control of the system more often, thereby improving performance. We use Reinforcement Learning with the reward function defined in Eq. 9 for online retraining.

As in initial training, we use the DDPG algorithm (with the same settings) for online retraining. When the NC outputs an unrecoverable action, the DM switches control to the BC, and the AM computes the (negative) reward for this action and adds it to a pool of training samples. As in [18], we found that reusing the pool of training samples (DDPG’s experience replay buffer) from initial training of the NC evolves the policy in a more stable fashion, as retraining samples gradually replace initial training samples in the pool. Another benefit of reusing the initial training pool is that retraining of the NC can start almost immediately, without having to wait for enough samples

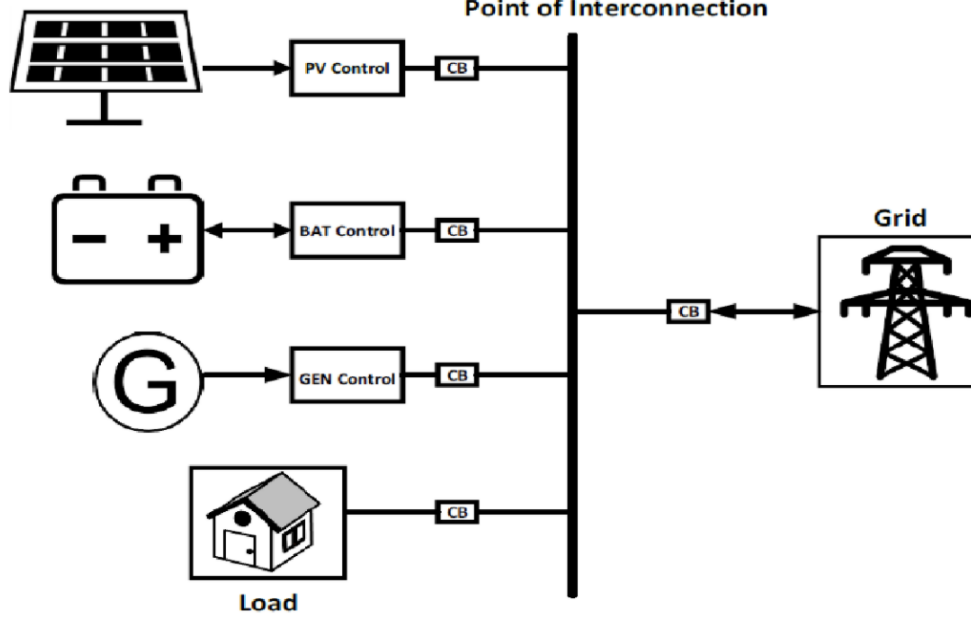


Figure 3: RTDS Microgrid Model [15]

to be collected online.

There are two methods to retrain the NC:

1. Off-policy retraining: At every time step while the BC is active, the BC’s action is used in the training sample. The reward for the BC’s action is based on the observed next state of the system.
2. Shadow-mode retraining: At every time step while the BC is active, the AM takes a sample by running the NC in shadow mode to compute its proposed action, and then simulates the behavior of the system for one time step to compute a reward for it.

In our experiments, both methods produce comparable benefits. Off-policy retraining is therefore preferable because it does not require simulation (or a dynamic model of the system) and hence is less costly.

7 Experimental Evaluation

We apply our SimpleMG methodology to a model of a microgrid [15] with three DERs: a battery, PV, and diesel generator. The three DERs are connected to the main grid via bus lines. As depicted in Fig. 3, the three DERs are connected to the main grid via bus lines. We are primarily interested in the PV control, since we apply SimpleMG to PV voltage regulation. The PV control includes multiple components, such as “three-phase to DQ0 voltage and current” transformer, average voltage and current control, power and voltage measurements, inner-loop dq current control, and outer-loop Maximum Power Point Tracking (MPPT) control. Our experimental evaluation of SimpleMG was carried out on RTDS, a high-fidelity power systems simulator.

We ran experiments for three configurations of the microgrid: Configuration 1: grid-connected mode with only the PV DER connected within the MG; Configuration 2: islanded mode with PV and diesel generator DERs connected within the MG; Configuration 3: islanded mode with PV, diesel generator, and battery (in discharging mode) DERs connected within the MG. All configurations also include a load. These configurations demonstrate SimpleMG’s ability to handle a wide variety of MG configurations involving various types of DERs. We did not perform experiments with the battery in charging mode, because in this mode, the battery is simply another load, and the configuration is equivalent to Configuration 1 or Configuration 2 with a larger load.

We use SimpleMG to ensure the safety property that the d -component of the output voltage of the inverter for the PV DER is within $\pm 3\%$ of the reference voltage $v_{ref} = 0.48$ kV. We adopted a 3% tolerance based on the discussion in [15]. SimpleMG could similarly be used to ensure additional desired safety properties. All experiments use runs of length 10 seconds, with the control period, RTDS time step, and simulation time step in MATLAB all equal to 3.2 milliseconds (msec), the largest time step allowed by RTDS.

7.1 Integration of SimpleMG in RTDS

The BC is the original droop controller described in [15], implemented in RTDS using components in the RTDS standard libraries. The DM is implemented as an RTDS *custom component* written in C. For an MG configuration, expressions for the BaC, λ and μ (see Section 4) are derived in MATLAB, converted to C data structures, and then included in a header file of the custom component. The BaCs are polynomials comprising 41, 67, and 92 monomials, respectively, for configurations 1, 2, and 3.

The NC is trained and implemented using Keras [5], a high-level neural network API written in Python, running on top of TensorFlow [1]. For training, we customized an existing skeleton implementation of DDPG in Keras, which we then used with the Adam optimizer [7]. Hyperparameters used during training involved a learning rate $lr = 0.0001$, discounting factor $\gamma = 0.99$, and target network update weight $\tau = 0.001$.

RTDS imposes limitations on custom components that make it difficult to implement complex NNs within RTDS. Existing NN libraries for RTDS, such as [12, 13], severely limit the NN’s size and the types of activation functions. Therefore, we implemented the NC external to RTDS, following the *software-defined microgrid control* approach in [29]. Fig. 4 shows our setup. We used RTDS’s GTNET-SKT communication protocol to establish a TCP connection between the NC running on a PC and an “NC-to-DM” relay component in the RTDS MG model. This relay component repeatedly sends the plant state to the NC, which computes its control action and sends it to the relay component, which in turn sends it to the DM.

Running the NC outside RTDS introduces control latency. We measured the round-trip time between RTDS and NC (including the running time of NC on the given state) to be 4.34 msec. Since the control period is 3.2 msec, each control action is delayed by one control period. The latency is mostly from network communication, since the PC running the NC was off-campus. We plan to reduce the latency by moving the NC to a PC connected to the same LAN as RTDS.

7.2 Consistency of RTDS and MATLAB Models

Our methodology requires an analytical model of the microgrid dynamics to derive a BaC for the BC and a switching condition for the DM. We therefore developed an analytical model in MATLAB

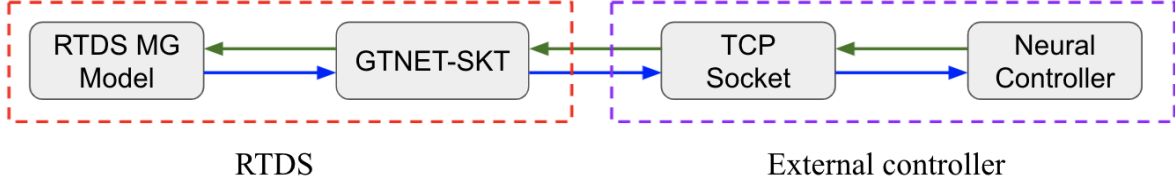


Figure 4: Integration of External NC with RTDS

Table 1: Voltage deviation (VD) and current deviation (CD) between output of PV DER in RTDS and MATLAB models

(a) Configuration 1				
	VD (kV)	VD (%)	CD (Amp)	CD (%)
Avg	0.000214	0.04	0.000129	0.028
Min	0.000187	0.03	0.000124	0.015
Max	0.000378	0.08	0.000181	0.036
(b) Configuration 2				
	VD (kV)	VD (%)	CD (Amp)	CD (%)
Avg	0.000348	0.07	0.000126	0.032
Min	0.000103	0.02	0.000104	0.019
Max	0.000493	0.10	0.000187	0.052
(c) Configuration 3				
	VD (kV)	VD (%)	CD (Amp)	CD (%)
Avg	0.001041	0.12	0.000238	0.047
Min	0.000119	0.02	0.000133	0.019
Max	0.001403	0.21	0.000187	0.102

based on the RTDS model and the description given in [15]. To verify consistency of MATLAB and RTDS models, we compared trajectories obtained from them under various operating conditions.

Table 1 reports deviations in output voltage and current trajectories of the PV DER between the two models under the control of the BC. The results are based on 100 trajectories starting from random initial states.

As expected, the two models are in close agreement. The small deviations are due to a few factors: (1) the RTDS model uses realistic dynamic models of transmission lines including their noise, whereas the MATLAB model ignores transmission line dynamics; and (2) the RTDS model uses average-value modeling to more efficiently simulate the dynamics in real-time [15], whereas in MATLAB, trajectories are calculated by solving ordinary differential equations of the dynamics at each simulation time-step.

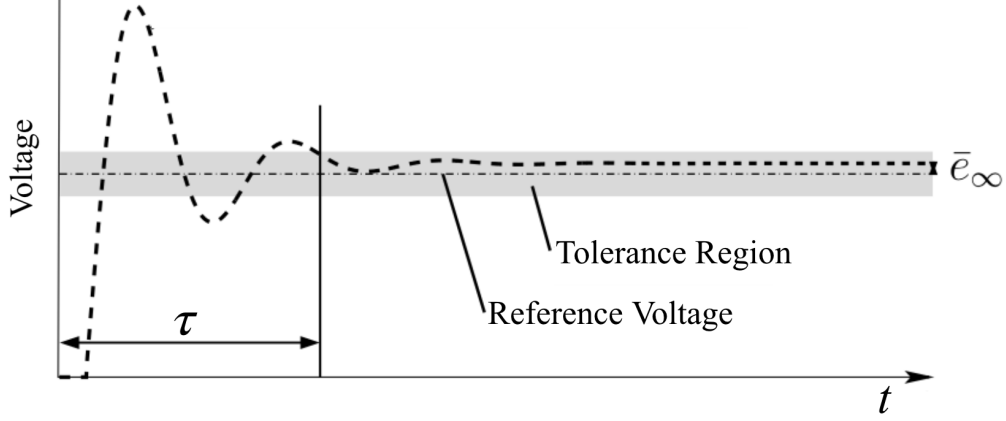


Figure 5: Schematic diagram showing tolerance region and mean absolute error \bar{e}_∞ [6]

7.3 Evaluation of Forward Switching Condition

We derive a BaC using the methodology presented in Section 3, and then derive a switching condition from the BaC, as described in Section 4. To find values of λ and μ , we use MATLAB’s `fmincon` function to solve the constrained optimization problems given in Eqs. 6 and 7.

An ideal FSC triggers a switch to the BC only if an unrecoverable state is actually reachable in one time step. For systems like microgrids with complex dynamics, switching conditions derived in practice are generally more conservative; i.e., the switch may occur a few time steps before that. To show that our FSC is not overly conservative, we performed experiments using an AC that continuously increases the voltage and hence soon violates safety. The PV voltage controller has two outputs, m_d and m_q , for the d and q components of the voltage, respectively. The dummy AC simply uses constant values for its outputs, with $m_d = 0.5$ and $m_q = 1e - 6$. These experiments were performed with PV DER in grid connected mode.

In 100 runs from random initial states and initial voltage in range [0.4752 kV, 0.4848 kV] with unsafe voltage and reference voltage at 0.4944 kV, 0.48 kV respectively, we measured mean initial voltage, mean voltage at switching, standard deviation of voltage switching, mean number of time steps before switching, percentage difference between mean voltage at switching and unsafe voltage to be at 0.47953942 kV, 0.49211286 kV, 0.0002314 kV, 127.4, 0.476% respectively. We also measured the mean total time steps for violation to occur in the absence of switching at 130.2 steps. Our FSC derived using a 4th-order Taylor approximation triggered a switch three time steps, on average, before a safety violation occurred. We get very close to unsafe voltage (within 0.476%) before switching occurs.

7.4 Evaluation of Neural Controller

The NC for a microgrid configuration is a DNN with four fully-connected hidden layers of 256 neurons each and one output layer. The hidden layers and output layer use the ReLU and tanh activation function, respectively. The NC is trained on 1 million samples (one-step transitions) from MATLAB simulations, processed in batches of 200. Transitions start from random states, with initial values uniformly sampled from [0, 1]. Training takes approximately 2 hours. The number of trainable parameters in the actor and critic networks are 198,672 and 149,111, respectively.

Table 2: Performance comparison of NC and BC

(a) Experimental Results for Configuration 1

Controller	CR	CT	$\sigma(CT)$	\bar{e}_∞	$\sigma(\bar{e}_\infty)$
NC	100	67.5	5.8	1.1e-4	1.0e-5
BC	100	102.3	8.2	4.2e-4	3.7e-5

(b) Experimental Results for Configuration 2

Controller	CR	CT	$\sigma(CT)$	\bar{e}_∞	$\sigma(\bar{e}_\infty)$
NC	100	76.8	6.1	1.3e-4	1.2e-5
BC	100	108.8	8.3	5.1e-4	3.8e-5

(c) Experimental Results for Configuration 3

Controller	CR	CT	$\sigma(CT)$	\bar{e}_∞	$\sigma(\bar{e}_\infty)$
NC	100	81.1	7.7	1.5e-4	1.3e-5
BC	100	115.7	9.8	5.8e-4	3.8e-5

The input state to the NN is $[i_d \ i_q \ i_{od} \ i_{oq} \ v_{od} \ v_{oq} \ i_{ld} \ i_{lq} \ u_d \ u_q]$, where i_d and i_q are the d - and q -components of the dq current measured at the local load of the inverter, i_{od} and i_{oq} are the d - and q -components of the output current of the inverter measured at point of coupling to the main grid, v_{od} and v_{oq} are the d - and q -components of the output voltage of the inverter measured at point of coupling to the main grid, i_{ld} and i_{lq} are the d - and q -components of the input current to the current controller, and u_d and u_q are the d - and q -components of the ground truth control action used to generate the next state.

We created an infrastructure for training the NC using samples from RTDS. The main challenge is setting the RTDS state to a starting state selected by the training algorithm. RTDS does not provide a native facility for this, and we needed to use different techniques and some custom components to set the states of different types of microgrid components. Training with samples from RTDS would yield a slightly higher-performing controller but would be significantly slower, due to the overhead of sending states back and forth between RTDS and the training algorithm running on a PC.

Performance We evaluate a controller’s performance based on three metrics: convergence rate (CR), the percentage of trajectories in which the DER voltage converges to the tolerance region $v_{ref} \pm \epsilon$; average convergence time (CT), the average time required for convergence of the DER voltage to the tolerance region; and mean absolute error (\bar{e}_∞) [6], the average deviation of the DER voltage from v_{ref} after the voltage enters the tolerance region. We always report CR as a percentage, CT in milliseconds, and \bar{e}_∞ in kV. Fig. 5 presents a schematic diagram of the DER voltage entering and staying within the tolerance region after τ time steps, and \bar{e}_∞ shows the difference between the actual voltage and the reference voltage.

We show that the NC outperforms the BC. For this experiment, we used RTDS to run the BC and NC starting from the same 100 initial states. Table 2 compares their performance, averaged

Table 3: Generalization performance of NC

(a) Experimental Results for Configuration 1					
	CR	CT	$\sigma(CT)$	\bar{e}_∞	$\sigma(\bar{e}_\infty)$
Gen 1	100	108.7	9.8	1.7e-4	1.5e-5
Gen 2	100	77.1	6.9	1.3e-4	1.1e-5
(b) Experimental Results for Configuration 2					
	CR	CT	$\sigma(CT)$	\bar{e}_∞	$\sigma(\bar{e}_\infty)$
Gen 1	100	118.2	10.1	2.1e-4	1.9e-5
Gen 2	100	81.2	6.2	1.5e-4	1.4e-5
(c) Experimental Results for Configuration 3					
	CR	CT	$\sigma(CT)$	\bar{e}_∞	$\sigma(\bar{e}_\infty)$
Gen 1	100	120.4	10.8	2.2e-4	1.9e-5
Gen 2	100	88.5	7.3	1.6e-4	1.4e-5

over 100 runs, with $\epsilon = 0.005$. We observe that for all three configurations, the NC outperforms the BC both in terms of average convergence time and mean absolute error. We also report the standard deviations (σ) for these metrics and note that they are small compared to the average values. The FSC was not triggered even once during these runs, showing that the NC is well-trained.

Generalization Generalization refers to the NC’s ability to perform well in contexts beyond the ones in which it was trained. First, we consider two kinds of generalization with respect to the microgrid state. Gen 1: the initial states of the DERs are randomly chosen from the range [1,2], instead of the range [0,1] used during training. Gen 2: the power set-point P^* is randomly chosen from the range [0.2, 1], whereas all training was done with $P^* = 1$. Table 3 presents the NC’s performance in these two cases, based on 100 runs for each case. We see that the NC performs well in both cases.

Second, we consider generalization with respect to the microgrid configuration. We perform two sets of experiment for this. Let NC- i denote the NC trained for Configuration i . In the first set of experiments, we test the performance of NC-1 for Configuration 2 and NC-2 for Configuration 1 on 100 runs from random initial states. In both cases, the CR was 100%. However, the mean absolute error for NC-1 was 4.7 times larger than when it was used with Configuration 1. The mean absolute error for NC-2 was 2.4 times larger than when it was used with Configuration 2. We conclude that an NC trained on a more complex microgrid generalizes better than one trained on a simpler microgrid.

In the second set of experiments, we evaluate how NC-1 and NC-2 handle dynamic changes to the microgrid configuration, even though no changes occurred during training. Each run starts with the PV and diesel generator DERs both connected, and the diesel generator DER disconnected after the voltage has converged. Both NCs succeed in continuously keeping the voltage in the tolerance region ($v_{ref} \pm \epsilon$) after the disconnection. The disconnection causes a slight drop in the subsequent

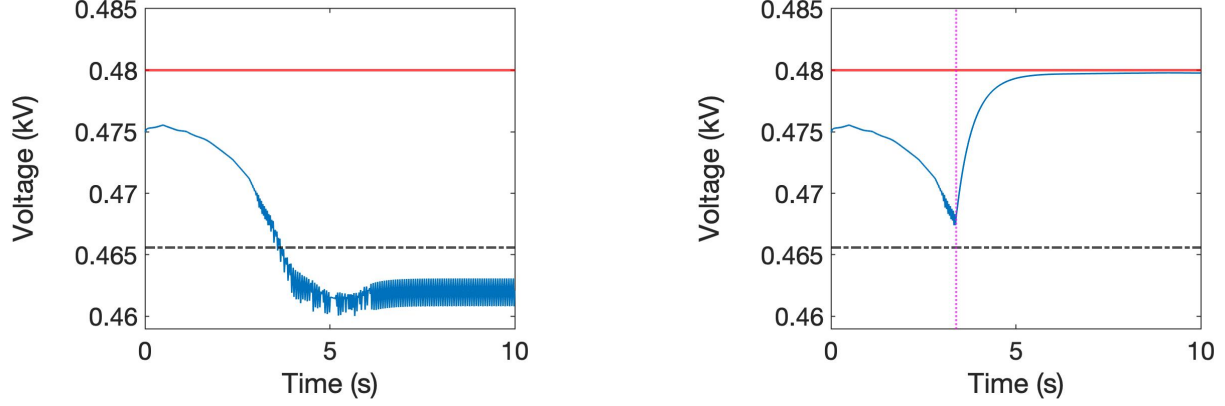


Figure 6: NC with adversarial inputs (left: without BC, right: with BC)

steady-state voltage, a drop of 0.195% for NC-1 and 0.182% for NC-2.

Adversarial input attacks We demonstrate that RL-based neural controllers are vulnerable to adversarial input attacks. We use the gradient-based attack algorithm described in Section 5 to generate adversarial inputs for our NCs. We use an adversarial attack constant $c = 0.05$ and the parameters for the beta distributions are $\alpha = 2$ and $\beta = 4$. From 100,000 unique initial states, we obtain 8, 6, and 5 adversarial states for Configurations 1, 2, and 3, respectively. In these experiments, we perturb all state variables simultaneously. In a real-life attack scenario, an attacker might have the capability to modify only a subset of them. Nevertheless, our experiments illustrate the fragility of RL-based neural controllers and the benefits of protecting them with NSA.

We confirmed with simulations that all generated adversarial states lead to safety violations when the NC alone is used, and that safety is maintained when SimpleMG is used. Fig. 6 (left) shows one such case, where the NC commits a voltage safety violation. The red horizontal line shows the reference voltage $v_{ref} = 0.48$ kV. The black dashed horizontal line shows the lower boundary of the safety region, 3% below v_{ref} . Fig. 6 (right) shows how SimpleMG prevents the safety violation. The pink dotted vertical line marks the switch from NC to BC.

We also confirmed that for all generated adversarial states, the forward switch is followed by a reverse switch. The time between forward switch and reverse switch depends on the choice of m (see Section 4.2). In the run shown in Fig. 6 (b), they are 5 time steps (0.016 sec) apart; the time of the reverse switch is not depicted explicitly, because the line for it would mostly overlap the line marking the forward switch. For $m = 2, 3, 4$ with Configuration 1, the average number of time steps between them are 7 (0.0244 sec), 11 (0.0352 sec), and 16 (0.0512 sec), respectively. For $m = 2, 3, 4$ with Configuration 2, the average time steps between them are 7 (0.0244 sec), 13 (0.0416 sec), and 17 (0.0544 sec), respectively. For $m = 2, 3, 4$ with Configuration 3, the average time steps between them are 8 (0.0256 sec), 14 (0.0448 sec), and 19 (0.0608 sec), respectively.

7.5 Evaluation of Adaptation Module

To measure the benefits of online retraining, we used the adversarial inputs described above to trigger switches to BC. For each microgrid configuration, we ran the original NC from the first adversarial state for that configuration, performed online retraining while the BC is in control, and

Table 4: Performance comparison of original NC and NC retrained by AM

(a) Experimental Results for Configuration 1					
NC	CR	CT	$\sigma(CT)$	\bar{e}_∞	$\sigma(\bar{e}_\infty)$
retrained	100	60.4	5.6	1.0e−4	1.0e−5
original	100	67.5	5.8	1.1e−4	1.0e−5

(b) Experimental Results for Configuration 2					
NC	CR	CT	$\sigma(CT)$	\bar{e}_∞	$\sigma(\bar{e}_\infty)$
retrained	100	69.4	5.3	1.1e−4	1.0e−5
original	100	76.8	6.1	1.3e−4	1.2e−5

(c) Experimental Results for Configuration 3					
NC	CR	CT	$\sigma(CT)$	\bar{e}_∞	$\sigma(\bar{e}_\infty)$
retrained	100	70.2	5.7	1.4e−4	1.3e−5
original	100	81.1	7.7	1.5e−4	1.3e−5

repeated this procedure for the remaining adversarial states for that configuration except starting with the updated NC from the previous step. As such, the retraining is cumulative for each configuration. We performed this entire procedure separately for different RSCs corresponding to different values of m . After the cumulative retraining, we ran the retrained controller from all of the adversarial states, to check whether the retrained NC was still vulnerable (i.e., whether those states still led to safety violations).

For Configuration 1, the BC was in control for a total of 56, 88, and 128 time steps for $m = 2, 3, 4$, respectively. For Configuration 2, the BC was in control for a total of 42, 78, and 102 time steps for $m = 2, 3, 4$, respectively. For Configuration 3, the BC was in control for a total of 40, 70, and 95 time steps for $m = 2, 3, 4$, respectively. For $m = 2$, the retrained controllers were still vulnerable to some adversarial states for each configuration. For $m = 3, 4$, the retrained controllers were not vulnerable to any of the adversarial states, and voltage always converged to the tolerance region.

Table 5 compares the performance of the original and retrained NCs for each configuration, averaged over 100 runs starting from random (non-adversarial) states. The retraining shows a slight improvement in the performance of the NC; thus, retraining improves both safety and performance.

A potential concern is whether with online retraining can be done in real-time; i.e., whether a new retraining sample can be processed within one control period, so the retrained NC is available as soon as the RSC holds. In the above experiments, run on a laptop with an Intel i5-6287U CPU, retraining is done nearly in real-time: on average, the retraining finishes 0.285 milliseconds (less than one-tenth of a control period) after the RSC holds.

8 Related Work

The use of BaCs in the Simplex architecture originated in [30]. There are, however, significant differences between their method for obtaining the switching condition and ours. Their switching

Table 5: Performance comparison of original NC and NC retrained by AM

NC	CR	CT	$\sigma(CT)$	\bar{e}_∞	$\sigma(\bar{e}_\infty)$
retrained	100	70.2	5.7	1.4e−4	1.3e−5
original	100	81.1	7.7	1.5e−4	1.3e−5

logic involves computing, at each decision period, the set of states reachable from the current state within one control period, and then checking whether that set of states is a subset of the zero-level set of the BaC. Our approach avoids the need for reachability calculations by using a Taylor approximation of the BaC, and bounds on the BaC’s derivatives, to bound the possible values of the BaC during the next control period and thereby determine recoverability of states reachable during that time. Our approach is computationally much cheaper: a reachability computation is expensive compared to evaluating a polynomial. Their framework can handle hybrid systems. Extending our method to hybrid systems is a direction for future work.

Mehmood et al. [14] propose a distributed Simplex architecture with BCs synthesized using control barrier functions (CBFs) and with switching conditions derived from the CBFs, which are BaCs satisfying additional constraints. A derivation of switching conditions based on Taylor approximation of CBFs is briefly described but does not consider the remainder error, admissible states, or restricted admissible states, and does not include a proof of correctness (which requires an analysis of the remainder error).

Kundu et al. [9] and Wang et al. [28] use BaCs for safety of microgrids, and Prajna et al. [22] propose an approach for stochastic safety verification of continuous and hybrid systems using BaCs. These approaches are based on the use of verified-safe controllers; they do not allow the use of unverified high-performance controllers, do not consider switching conditions, etc.

The application of neural networks for microgrid control is gaining in popularity [11]. Amoateng et al. [2] use adaptive neural networks and cooperative control theory to develop microgrid controllers for inverter-based DERs. Using Lyapunov analysis, they prove that their error-function values and weight-estimation errors are uniformly ultimately bounded. Tan et al. [26] use Recurrent Probabilistic Wavelet Fuzzy Neural Networks (RPWFNNs) for microgrid control, since they work well under uncertainty and generalize well. We used more traditional DNNs, since they are already high performing, and our focus is on safety assurance. Our SimpleMG framework, however, allows any kind of neural network to be used as the AC and can provide the safety guarantees lacking in their work. Unlike our approach, none of these works provide safety guarantees.

9 Conclusion

We have presented *SimpleMG*, a new, provably correct design methodology for runtime assurance of microgrids under real-time neural control. We used barrier certificates (BaCs) to establish SimpleMG’s runtime-assurance guarantees. In particular, we showed how to derive BaCs for traditional microgrid controllers and their associated safety properties, and we developed a new methodology to derive verified-safe forward switching conditions from BaCs. We also demonstrated how to train high-performance neural controllers (NCs).

We conducted an extensive experimental evaluation of SimpleMG using RTDS. Our evaluation, centered around a realistic microgrid model with three DERs, confirms that SimpleMG can be used

to develop high-performance, generalizable NCs while assuring specified safety properties, even in the presence of adversarial input attacks on the NC. We also ran experiments demonstrating that the derived FSCs switch control from the NC to the BC only a short time before a safety violation becomes unavoidable, and that online retraining of the NC is effective in preventing subsequent safety violations by the NC.

For future work, we will investigate other techniques for obtaining BaCs, including synthesis of BaC using NNs [32]. To eliminate the need for a dynamic model of the MG, we plan to explore: (i) learning neural ODEs [4, 33] that capture the MG dynamics, and (ii) deriving BaCs and switching conditions from said dynamics. We also plan to extend our approach to networked microgrids [31].

References

- [1] Abadi, M., et al.: TensorFlow: Large-scale machine learning on heterogeneous systems (2015), <https://www.tensorflow.org/>
- [2] Amoateng, D.O., Al Hosani, M., Elmoursi, M.S., Turitsyn, K., Kirtley, J.L.: Adaptive voltage and frequency control of islanded multi-microgrids. *IEEE Transactions on Power Systems* **33**(4), 4454–4465 (2018)
- [3] Anghel, M., Milano, F., Papachristodoulou, A.: Algorithmic construction of lyapunov functions for power system stability analysis. *IEEE Transactions on Circuits and Systems I: Regular Papers* **60**(9), 2533–2546 (2013)
- [4] Chen, T.Q., Rubanova, Y., Bettencourt, J., Duvenaud, D.: Neural ordinary differential equations. In: *Advances in Neural Information Processing Systems 31: Annual Conference on Neural Information Processing Systems (NeurIPS 2018)*. pp. 6572–6583 (2018)
- [5] Chollet, F., et al.: Keras (2015), <https://github.com/keras-team/keras.git>
- [6] Hafner, R., Riedmiller, M.: Reinforcement learning in feedback control. *Machine Learning* **84**(1-2), 137–169 (2011)
- [7] Kingma, D.P., Ba, J.: Adam: A method for stochastic optimization. In: *3rd International Conference on Learning Representations, ICLR 2015, San Diego, CA, USA, May 7-9, 2015, Conference Track Proceedings* (2015)
- [8] Krishnamurthy, S., Jahns, T.M., Lasseter, R.H.: The operation of diesel gensets in a CERTS microgrid. In: *2008 IEEE Power and Energy Society General Meeting - Conversion and Delivery of Electrical Energy in the 21st Century*. pp. 1–8 (2008)
- [9] Kundu, S., Geng, S., Nandanoori, S.P., Hiskens, I.A., Kalsi, K.: Distributed barrier certificates for safe operation of inverter-based microgrids. In: *2019 American Control Conference (ACC)*. pp. 1042–1047 (2019)
- [10] Lillicrap, T.P., Hunt, J.J., Pritzel, A., Heess, N., Erez, T., Tassa, Y., Silver, D., Wierstra, D.: Continuous control with deep reinforcement learning. In: *ICLR* (2016)
- [11] Lopez-Garcia, T.B., Coronado-Mendoza, A., Domínguez-Navarro, J.A.: Artificial neural networks in microgrids: A review. *Engineering Applications of Artificial Intelligence* **95**, 103894 (2020)

- [12] Luitel, B., Venayagamoorthy, G.K.: Neural networks in RSCAD for intelligent real-time power system applications. In: 2013 IEEE Power Energy Society General Meeting. pp. 1–5 (2013)
- [13] Luitel, B., Venayagamoorthy, G.K., Oliveira, G.: Developing neural networks library in RSCAD for real-time power system simulation. In: 2013 IEEE Computational Intelligence Applications in Smart Grid (CIASG). pp. 130–137 (2013)
- [14] Mehmood, U., Stoller, S.D., Grosu, R., Roy, S., Damare, A., Smolka, S.A.: A distributed simplex architecture for multi-agent systems. In: Proceedings of the Symposium on Dependable Software Engineering: Theories, Tools and Applications (SETTA 2021). Lecture Notes in Computer Science, vol. 13071. Springer (2021)
- [15] Nzimako, O., Rajapakse, A.: Real time simulation of a microgrid with multiple distributed energy resources. In: 2016 International Conference on Cogeneration, Small Power Plants and District Energy (ICUE). pp. 1–6 (2016)
- [16] O’Rourke, C.J., Qasim, M.M., Overlin, M.R., Kirtley, J.L.: A geometric interpretation of reference frames and transformations: dq0, Clarke, and Park. *IEEE Transactions on Energy Conversion* **34**(4), 2070–2083 (2019)
- [17] Pattanaik, A., Tang, Z., Liu, S., Bommanan, G., Chowdhary, G.: Robust deep reinforcement learning with adversarial attacks (2017)
- [18] Phan, D., Grosu, R., Jansen, N., Paoletti, N., Smolka, S.A., Stoller, S.D.: Neural simplex architecture. In: NASA Formal Methods Symposium (2020)
- [19] Pogaku, N., Prodanovic, M., Green, T.C.: Modeling, analysis and testing of autonomous operation of an inverter-based microgrid. *IEEE Transactions on Power Electronics* **22**(2), 613–625 (2007)
- [20] Prajna, S.: Barrier certificates for nonlinear model validation. *Automatica* **42**(1), 117–126 (2006)
- [21] Prajna, S., Jadbabaie, A.: Safety verification of hybrid systems using barrier certificates. In: Alur, R., Pappas, G.J. (eds.) Proceedings of the 7th International Workshop on Hybrid Systems: Computation and Control (HSCC 2004). Lecture Notes in Computer Science, vol. 2993, pp. 477–492. Springer (2004)
- [22] Prajna, S., Jadbabaie, A., Pappas, G.J.: A framework for worst-case and stochastic safety verification using barrier certificates. *IEEE Transactions on Automatic Control* **52**(8), 1415–1428 (2007)
- [23] RTDS Technologies Inc.: Real-time digital simulation for the power industry, Manual set
- [24] Seto, D., Krogh, B., Sha, L., Chutinan, A.: The simplex architecture for safe online control system upgrades. In: Proceedings of the 1998 American Control Conference. ACC (IEEE Cat. No. 98CH36207). vol. 6, pp. 3504–3508 (1998)
- [25] Sha, L.: Using simplicity to control complexity. *IEEE Software* **18**(4), 20–28 (2001)

- [26] Tan, K.H., Lin, F.J., Shih, C.M., Kuo, C.N.: Intelligent control of microgrid with virtual inertia using recurrent probabilistic wavelet fuzzy neural network. *IEEE Transactions on Power Electronics* **35**(7), 7451–7464 (2020)
- [27] Ton, D.T., Smith, M.A.: The U.S. department of energy’s microgrid initiative. *The Electricity Journal* **25**(8), 84–94 (2012)
- [28] Wang, L., Han, D., Egerstedt, M.: Permissive barrier certificates for safe stabilization using sum-of-squares. In: 2018 Annual American Control Conference (ACC). pp. 585–590 (2018)
- [29] Wang, L., Qin, Y., Tang, Z., Zhang, P.: Software-defined microgrid control: The genesis of decoupled cyber-physical microgrids. *IEEE Open Access Journal of Power and Energy* **7**, 173–182 (2020)
- [30] Yang, J., Islam, M.A., Murthy, A., Smolka, S.A., Stoller, S.D.: A simplex architecture for hybrid systems using barrier certificates. In: Proceedings of the 36th International Conference on Computer Safety, Reliability, and Security (SAFECOMP 2017). Lecture Notes in Computer Science, vol. 10488. Springer (2017)
- [31] Zhang, P.: Networked Microgrids. Cambridge University Press (2021)
- [32] Zhao, H., Zeng, X., Chen, T., Liu, Z.: Synthesizing barrier certificates using neural networks. In: Proceedings of the 23rd International Conference on Hybrid Systems: Computation and Control (HSCC ’20) (2020)
- [33] Zhou, Y., Zhang, P.: Neuro-reachability of networked microgrids. *IEEE Transactions on Power Systems* (2021)